Journal of
Synchrotron
Radiation

ISSN 1600-5775

Received 7 September 2013
Accepted 27 January 2014

© 2014 International Union of Crystallography

Correction method for the self-absorption effects in fluorescence extended X-ray absorption fine structure on multilayer samples

Wen-Bin Li,[a] Xiao-Yue Yang,[a] Jing-Tao Zhu,[a] Yu-Chun Tu,[a] Bao-Zhong Mu,[a] Hai-Sheng Yu,[b] Xiang-Jun Wei,[b] Yu-Ying Huang[b] and Zhan-Shan Wang[a]*

[a]MOE Key Laboratory of Advanced Micro-structured Materials, Institute of Precision Optical Engineering (IPOE), School of Physics Science and Engineering, Tongji University, Shanghai 200092, People's Republic of China, and [b]Shanghai Institute of Applied Physics, Chinese Academy of Science, Shanghai 201204, People's Republic of China. *E-mail: wangzs@tongji.edu.cn

A novel correction method for self-absorption effects is proposed for extended X-ray absorption fine structure (EXAFS) detected in the fluorescence mode on multilayer samples. The effects of refraction and multiple reflection at the interfaces are fully considered in this correction method. The correction is performed in *k*-space before any further data analysis, and it can be applied to single-layer or multilayer samples with flat surfaces and without thickness limit when the model parameters for the samples are known. The validity of this method is verified by the fluorescence EXAFS data collected for a Cr/C multilayer sample measured at different experimental geometries.

Keywords: EXAFS; self-absorption effects; multilayer; X-ray fluorescence; XRR; scattering factors.

1. Introduction

Extended X-ray absorption fine structure (EXAFS) detected in the fluorescence mode is a powerful method for determining the local atomic structure around a specific element within samples, especially for the samples which are unsuitable for measurements in the transmission mode. As pointed out firstly by Jaklevic *et al.* (1977), the fluorescence intensity measured in fluorescence EXAFS is directly proportional to the absorption coefficient of a central atom of interest for dilute and thin samples. However, the fluorescence EXAFS may be susceptible to the self-absorption effects depending on the concentration of the atom of interest, the sample thickness and the experimental geometry (Jiang & Crozier, 1998; Meirer *et al.*, 2008). The self-absorption effects can cause a damping and broadening of the oscillating structures of the absorption coefficient, which thus produce errors on the determined local atomic structures, such as coordination numbers and Debye–Waller factors. In order to avoid or minimize the self-absorption effects, it has been suggested that fluorescence EXAFS can be measured at grazing-exit geometry (Pease *et al.*, 1989; Suzuki, 1989; Brewe *et al.*, 1994; Hayakawa *et al.*, 1991). For this experimental geometry, fluorescence EXAFS has the advantage of surface sensitivity instead of bulk sensitivity for detecting local atomic structures. Recently, Achkar *et al.* (2011) proposed a novel approach to measure X-ray absorption spectroscopy free from self-absorption effects by detecting a non-resonant X-ray emission spectrum from a different element than the probed one. However, this approach has not been demonstrated in the hard X-ray regime up to now.

For fluorescence EXAFS experiments where the self-absorption effects cannot be avoided, a correction method has to be used on the measured fluorescence spectra in order to recover the true EXAFS signal $\chi(k)$. Most of the correction methods have been based on a well known and simple fluorescence intensity expression [see, for example, equation (1) of Pease *et al.* (1989)], where concentrated single-layer film samples having large (Tröger *et al.*, 1992; Eisebitt *et al.*, 1993; Pfalzer *et al.*, 1999; Tan *et al.*, 1989; Carboni *et al.*, 2005) or intermediate thickness (Booth & Bridges, 2005) have been considered. For multilayer samples, few correction methods (Castañer & Prieto, 1997; Meyer *et al.*, 2000; Heald *et al.*, 1988) have been proposed to correct for the self-absorption effects. Castañer & Prieto (1997) provided a method by regarding a multilayer as a single layer after considering the information depth of fluorescence yield. However, this correction method did not consider the effects of refraction and multi-reflection when the incident X-rays penetrated through the multilayer samples. Meyer *et al.* (2000) also proposed an approximate method to correct for the self-absorption effects by using effective absorption coefficients determined from the integral electric field intensities of different layers. Different from other correction methods, Heald *et al.* (1988) developed a method to make corrections directly on coordination numbers and Debye–Waller factors. Since no convenient correction

methods have been provided for multilayers, the application of the fluorescence EXAFS approach on characterizing multilayer samples is hindered to some extent. In this paper, a novel correction method based on the formalism of fluorescence intensity calculation is presented to correct for the self-absorption effects directly in k-space for single-layer or multilayer samples. For this method, the effects of refraction and multi-reflection between neighboring layers have been considered. Additionally, interface roughnesses, which affect the X-ray field intensity distributions inside multilayers, have also been considered in this method. This correction method is demonstrated by comparing the corrected Cr $K\alpha$ fluorescence EXAFS data of a Cr/C multilayer measured at different geometries. This paper is organized as follows. §2 presents the experimental conditions and the experimental results. The basic theory for the fluorescence intensity calculation is given in §3. In §4 the correction method is described and the corrected experimental results are presented. Finally, §5 gives a brief summary.

2. Experiments

The EXAFS experiments were performed at the BL14W1 beamline (BL14W1@SSRF, 2009) of Shanghai Synchrotron Radiation Facility (SSRF) with an electron beam energy of 3.5 GeV and an average current of 220 mA. This beamline provided a focused X-ray beam from 4 to 22.5 keV with a photon flux of about 10^{13} photons s^{-1} (at 10 keV). Synchrotron radiation X-rays were monochromated with a Si(111) double-crystal monochromator and focused by a focusing mirror after the monochromator. In the experiments, we could not measure a reference sample for energy calibration in parallel with the Cr/C multilayer sample under investigation. Therefore, the photon energy was calibrated by a standard Cr metal foil before the experiments started. As shown in Fig. 1, the focused X-ray beam was collimated by two slits before an ionization chamber, which was used to monitor the incident beam intensity. On the sample stage, the Cr/C multilayer sample was mounted on a sample holder with a beam size of ~0.4 mm × 0.2 mm. The sample holder with multiple axes of movement can be rotated to vary the grazing-incidence angle θ with respect to the sample surface. As illustrated in Fig. 1, a 32-element Ge solid-state detector array cooled with liquid nitrogen was used to collect the emitted X-ray fluorescence photons in the orbit plane at 90° with respect to the incident beam.

In this study, a periodic multilayer sample of $[Cr(20.0\ nm)/C(10.0\ nm)]_5$ was deposited onto a polished silicon wafer(100) of size 20 mm × 15 mm using the direct-current magnetron sputtering method. Before deposition, the base pressure inside the chamber was better than 2.0×10^{-4} Pa. During deposition, argon gas with a purity of 99.99% was used as the sputtering gas and the working pressure was kept at about 0.13 Pa. For correcting the self-absorption effects, the actual model parameters for the multilayer sample are required, which include the layer materials, thickness, density and interface roughness. For this purpose, the grazing-incidence X-ray reflectivity measurements were carried out in θ–2θ geometry mode using an X-ray diffractometer (D1 system, Bede Ltd), which worked at a photon energy of 8.046 keV (Cu $K\alpha$ line) well away from the EXAFS data region of the Cr K-edge. For obtaining the actual model parameters of the multilayer, the measured X-ray reflectivity (XRR) curve was fitted using Bede *Refs* software with a genetic algorithm (Wormington *et al.*, 1999). During the fitting processes, the number of layers in the multilayer was a fixed input parameter. As shown in Fig. 2, the fitted results agree quite well with the experimental data, which provide the average thickness, interface roughness and density of the Cr layer, d_{Cr} = 20.08 nm, σ_{Cr} = 0.44 nm and ρ_{Cr} = 7.60 g cm^{-3}, respectively, as well as that of the C layer, d_C = 10.63 nm, σ_C = 0.52 nm and ρ_C = 2.38 g cm^{-3}, respectively. These model parameters were further used as input parameters for calculating the Cr $K\alpha$ fluorescence intensity in the EXAFS energy region in order to correct for the self-absorption effects.

In this experiment, Cr $K\alpha$ fluorescence EXAFS spectra of the Cr/C multilayer were measured at five different angles of θ, 3.0°, 5.0°, 10.0°, 30.0° and 45.0°, with the same acquisition time. In order to show the effects of different experimental geometries on the measured results, the fluorescence spectra

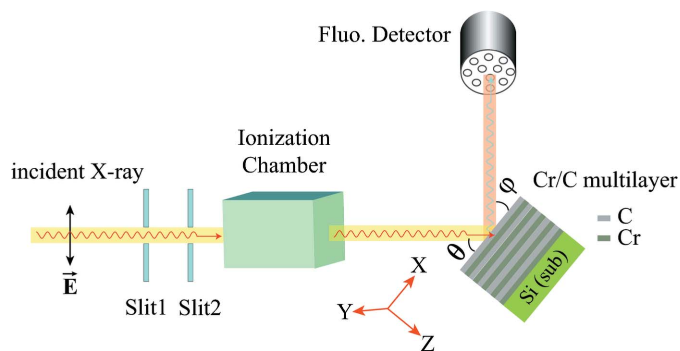

Figure 1
Schematic of the experimental set-up for the fluorescence EXAFS measurement. The angles of θ and φ represent the incident X-ray beam and the detected X-ray fluorescence photon direction with respect to the sample surface, respectively.

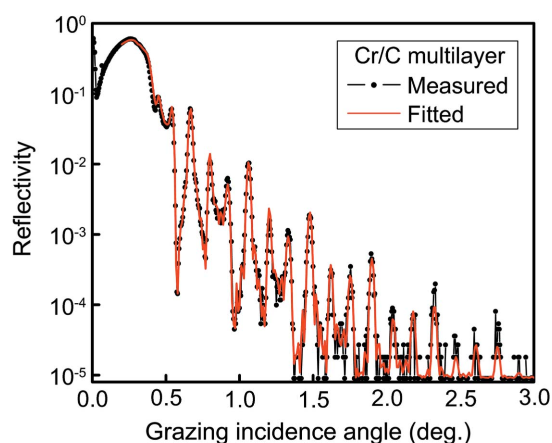

Figure 2
Measured and fitted grazing-incidence X-ray reflectivity curves for the multilayer sample $Si(Sub)/[Cr/C]_5$.

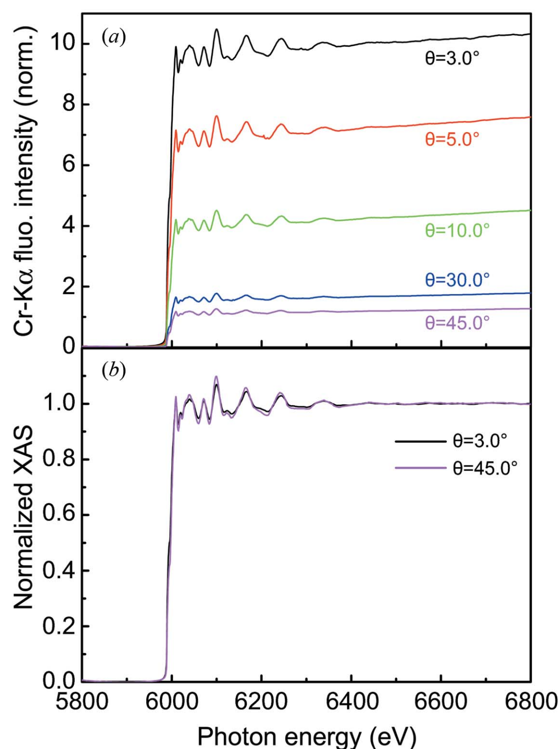

Figure 3
(a) Cr $K\alpha$ fluorescence spectra of the Cr/C multilayer sample normalized by the incident beam intensity at different grazing-incidence angles. (b) X-ray absorption spectra normalized to the edge jump at θ = 3.0° and 45.0°.

normalized by the corresponding-incident X-ray photon flux are given in Fig. 3(a). As seen in Fig. 3(a), the fluorescence spectrum measured at a smaller grazing incidence angle has a higher counting rate, which is mainly due to the fact that the fluorescence intensity is proportional to the illuminated sample area detected by the fluorescence detector. So, one advantage of measuring the fluorescence EXAFS at a relatively small grazing-incidence angle is that higher statistics can be acquired with the same acquisition time. However, the measurement at this experimental geometry may suffer from severe self-absorption effects compared with the measurement at a large grazing-incidence angle. In Fig. 3(b), X-ray absorption spectra normalized to the edge jumps are shown for the measurements at grazing-incidence angles of 3.0° and 45.0°. A strong damping of the experimental EXAFS amplitudes at θ = 3.0° with respect to the spectrum at θ = 45.0° can be clearly identified.

Fig. 4 gives the experimental EXAFS signals $k\chi(k)$ extracted from the fluorescence spectra of Fig. 3(a) using the *Athena* interface to the *IFEFFIT* program package (Ravel & Newville, 2005) according to a standard data analysis procedure. Owing to the self-absorption effects, the damping of the experimental EXAFS amplitudes is clearly observed for this sample (total thickness of Cr layer ~100 nm) at grazing-incidence angles of 3.0°, 5.0° and 10.0°. Additionally, the self-absorption effects become more severe when the grazing-incidence angle becomes smaller. At angles of 30.0° and 45.0°, the experimental EXAFS data have almost the same amplitudes, which demonstrates that the self-absorption effects are negligible at angles larger than 30.0° for this specific sample. For obtaining the true EXAFS signal $\chi(k)$, a correction method is needed for the measured fluorescence spectrum when the self-absorption cannot be ignored for single-layer or multilayer samples.

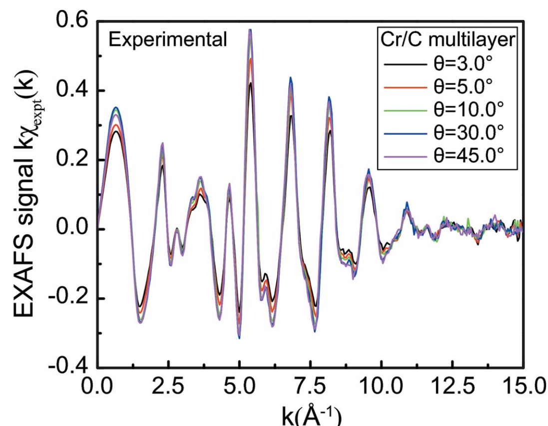

Figure 4
Experimental fluorescence EXAFS $k\chi(k)$ at the Cr K-edge for the Cr/C multilayer sample. The self-absorption effects are demonstrated by the damping of the EXAFS amplitudes at small grazing-incidence angles.

3. Theory background

Since this correction method is based on XRR and X-ray fluorescence intensity analysis, we briefly review the theoretical background (Parratt, 1954; Windt, 1998; de Boer, 1991; Ghose & Dev, 2001) for the calculation of XRR and the fluorescence intensity for a multilayer. As done in this experiment, a plane electromagnetic wave with p polarization is considered impinging on a multilayer, which consists of N layers of thin-film structures deposited on an infinitely thick substrate. The jth layer of the multilayer has a refractive index of n_j and thickness of d_j with surface roughness of σ_j. In the X-ray energy regime, it is common practice to write the refractive index in the following form,

$$n = 1 - \delta - i\beta, \tag{1}$$

where δ is the deviation term of the real part of the refractive index from unity and β represents the absorption of X-rays inside the medium. Both terms are related to the atomic scattering factors of the individual atoms by the formula (Henke *et al.*, 1993)

$$\delta = \frac{r_e \lambda^2}{2\pi} \sum_i N_i \left(Z_i + f_i'\right), \tag{2}$$

$$\beta = \frac{r_e \lambda^2}{2\pi} \sum_i N_i f_i'' = \frac{\lambda}{4\pi} \mu, \tag{3}$$

where $r_e = e^2/m_e c^2$ is the classical electron radius and λ is the wavelength of the incident X-rays. N_i is the number of atoms of type i with atomic number Z_i per unit volume. μ represents the absorption coefficient of the medium. The energy-depen-

dent terms of f_i' and f_i'' represent the real and imaginary anomalous dispersion factors of atoms of type i, respectively. The wavevector of the plane electromagnetic wave in the jth layer, $k_j = k_j' - ik_j''$, can be given in the XZ plane by

$$k_{j,x} = (2\pi/\lambda)\cos\theta, \quad k_{j,z} = (2\pi/\lambda)\left(\varepsilon_j - \cos^2\theta\right)^{1/2}. \quad (4)$$

θ is the grazing incidence angle with respect to the sample surface, and $\varepsilon_j = n_j^2 \approx 1 - 2\delta_j - i2\beta_j$ is the complex dielectric constant of the jth layer medium. The electric field amplitude of the plane wave with frequency ω in layer j at position $\mathbf{r}$ can be written as

$$E_j(\mathbf{r}) = E_j \exp\left(-ik_{j,z}z\right)\exp\left[i\left(\omega t - k_{j,x}x\right)\right], \quad (5)$$

where E_j is the field amplitude at the top of layer j. For calculating the electric field intensity distribution inside the multilayer, the amplitudes of transmitted and reflected X-ray fields at the top of layer j should be determined beforehand. Considering an X-ray wave with p polarization incident on a smooth interface, the complex coefficients of reflection r_j and transmission t_j are given by Fresnel's formulae

$$r_j = \frac{n_{j+1}^2 k_{j,z} - n_j^2 k_{j+1,z}}{n_j^2 k_{j+1,z} + n_{j+1}^2 k_{j,z}}, \quad t_j = \frac{2n_j n_{j+1} k_{j,z}}{n_j^2 k_{j+1,z} + n_{j+1}^2 k_{j,z}}. \quad (6)$$

According to actual conditions, the roughnesses of interfaces and substrate surface cause a loss of specular reflectance, so the Fresnel coefficients are needed to be modified. There is a practical method (de Boer, 1991) where the coefficient r_j is multiplied by a factor S_j and the coefficient t_j is multiplied by a factor T_j,

$$S_j = \exp\left[-2\sigma_j^2 k_{j,z}k_{j+1,z}\right], \quad T_j = \exp\left[\sigma_j^2\left(k_{j,z} - k_{j+1,z}\right)^2/2\right]. \quad (7)$$

The amplitudes of transmitted (E_j^t) and reflected (E_j^r) X-ray fields at the top of layer j can be obtained by using the following relations,

$$E_j^r = a_j^2 X_j E_j^t, \quad E_{j+1}^t = \frac{a_j E_j^t t_j T_j}{1 + a_{j+1}^2 X_{j+1} r_j S_j}, \quad X_j = \frac{\left(r_j S_j + a_{j+1}^2 X_{j+1}\right)}{1 + a_{j+1}^2 X_{j+1} r_j S_j}, \quad a_j = \exp\left(-ik_{j,z}d_j\right). \quad (8)$$

The calculation for X_j is performed in reverse order from the bottom to the top, where $E_s^r = X_s = 0$ because there is no reflection for the substrate. Then E_j^t and E_j^r are calculated for each layer from the top to the bottom, where the incident electric field E_0^t is normalized to have unit amplitude.

After obtaining the transmitted and reflected X-ray field amplitudes of E_j^t and E_j^r, the average X-ray field intensity $I_j(\theta, z)$ in the jth layer at depth z can be given by (Ghose & Dev, 2001)

$$I_j(\theta, z) = \left|E_j^t\right|^2\left\{\exp\left(-2k_{j,z}''z\right) + \left|\left(E_j^r/E_j^t\right)\right|^2\exp\left(2k_{j,z}''z\right) + 2\left|\left(E_j^r/E_j^t\right)\right|\cos\left[\nu(\theta) + 2k_{j,z}'z\right]\right\}, \quad (9)$$

where $\nu(\theta)$ is the phase of the ratio of reflected and transmitted electric fields $E_j^r/E_j^t = |E_j^r/E_j^t|\exp[i\nu(\theta)]$. Based on the fundamental parameter approach (Ghose & Dev, 2001), the total fluorescence intensity $F_x(E, \theta)$ emitted from an element x inside the multilayer can be expressed as

$$F_x(E,\theta) = \sum_{j=1}^{n} F_{j,x}(E,\theta) = \sum_{j=1}^{n} S_{x,E}\exp\left[-\sum_{n=1}^{j-1}\frac{(\mu/\rho)_{n,E_f}\rho_n d_n}{\sin\varphi}\right] \times \int_0^{d_j} C_{j,x}(z)\, I_j(\theta, z)\exp\left\{-\left[\frac{(\mu/\rho)_{j,E_f}}{\sin\varphi}\right]\rho_j z\right\}\mathrm{d}z. \quad (10)$$

Here $F_{j,x}(E,\theta)$ represents the contribution of fluorescence intensity emitted from the jth layer, which is corrected by the first exponent factor due to the attenuation effects when the fluorescence radiation travels through the upper layers to a detector. φ is the emission angle of the fluorescence radiation with respect to the sample surface. In this study, φ was approximately equal to $\pi/2 - \theta$. $(\mu/\rho)_{j,E_f}$ represents the mass attenuation coefficient of layer j for the detected fluorescence radiation with a characteristic energy of E_f. $S_{x,E}$ is the X-ray fluorescence production cross section for element x at the incident photon energy of E (de Boer, 1991; Tiwari *et al.*, 2010; LI *et al.*, 2012). $C_{j,x}$ and ρ_j are the mass fraction of element x and the density of layer j, respectively. Equation (10) gives the intensity of X-ray fluorescence photons emitted at the angle φ with respect to sample surfaces. For a fluorescence detector with a large solid angle, one should integrate over the solid angle subtended by the detector, which is especially important for grazing-exit geometry experiments (Brewe *et al.*, 1994). For this study, the acceptance angle of the fluorescence detector covered about $\Delta\theta = 5°$. However, it was found by simulations and experiments that this small solid angle had negligible effects on the measured EXAFS spectra due to the large exit angles used in this experiment. Therefore, the correction of the detector solid angle was ignored in this study.

For a given sample, the X-ray fluorescence intensity and the EXAFS spectrum can be simulated based on equations (9) and (10) when the model parameters of the sample are known already. During an energy scan in the EXAFS oscillation region, the absorption coefficient $\mu(E)$ wiggles up and down, which results in the decrease and increase of the penetration depth of the incident X-rays. A varied penetration depth means a varied excitation volume, from which the fluorescence photons are emitted (Meirer *et al.*, 2008). Therefore, the oscillation structures of the absorption coefficient are damped due to the self-absorption effects, which can be simulated by using the formalism mentioned above. In this formalism, the effects of refraction and multi-reflection between neighboring layers as well as the interface roughness have been considered, which have usually been absent in previous correction methods (Meyer *et al.*, 1995, 2000).

4. Correction method

In a fluorescence EXAFS experiment, if the fluorescence intensity is proportional to the absorption coefficient of an element of interest, the real interference function $\chi(E)$ can be extracted after a normalization procedure using the following expression,

$$\chi(E) = \frac{\mu(E) - \mu_0(E)}{\mu_0(E)} \approx \frac{I(E) - I_0(E)}{\Delta I_0(E_0)}, \qquad (11)$$

where $\mu(E)$ and $I(E)$ represent the absorption coefficient and the normalized fluorescence intensity of the detected atom inside a sample. $\mu_0(E)$ and $I_0(E)$ represent the absorption coefficient and the normalized fluorescence intensity of an isolated atom. $\Delta I_0(E_0)$ is the jump step at the absorption edge of E_0. Owing to self-absorption effects, the oscillatory function obtained in the fluorescence EXAFS experiment may be damped. In such a case, the experimentally determined EXAFS function $\chi_{\rm expt}(E)$ may be corrected as

$$\chi_{\rm corr}(E) = \chi_{\rm expt}(E)[1 + \alpha(E)], \qquad (12)$$

where $\chi_{\rm corr}(E)$ and $\chi_{\rm expt}(E)$ represent the corrected and experimental EXAFS functions, respectively. The energy-dependent function $\alpha(E)$ represents the correction factor needed to be determined. For this correction method, the correction factor $\alpha(E)$ is evaluated using an iterative procedure by comparing the experimental EXAFS function $\chi_{\rm expt}(E)$ with a calculated result $\chi_{\rm cal}(E)$, for which the calculation is performed based on the fluorescence intensity formalism as given in §3. A flow diagram of the correction procedure for multilayer samples is shown in Fig. 5. The proposed correction method comprises the following steps:

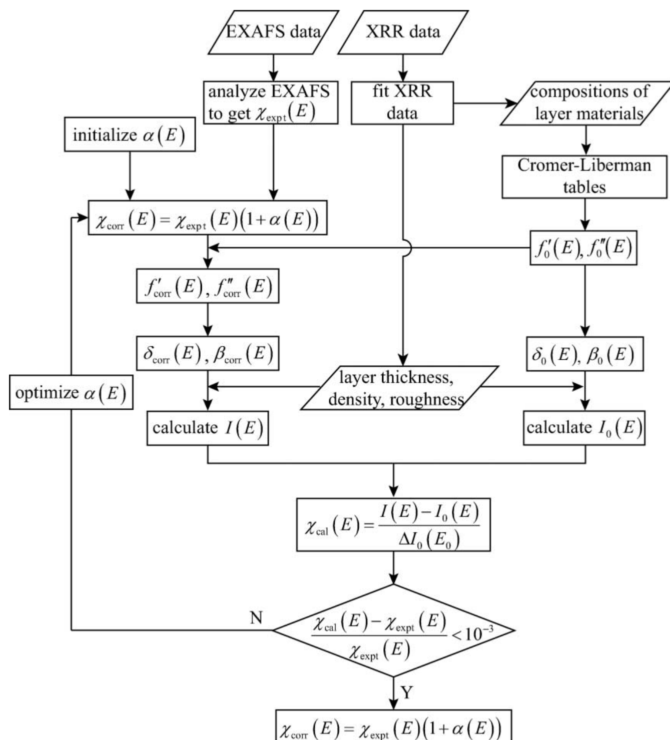

Figure 5
Basic flowchart of the correction procedure for the self-absorption effects of the fluorescence EXAFS on multilayer samples.

(i) Determining the model parameters of the sample (namely, the layer materials, thickness, density and roughness) by fitting XRR curve.

(ii) Calculating the fluorescence intensity $I_0(E)$ without oscillation structures. Based on the fundamental parameter approach, the fluorescence intensity $I_0(E)$ is calculated using the parameters of layer thickness, density, roughness and the refractive indices (δ_0, β_0) of the layer materials. The refractive indices δ_0 and β_0 are computed using atomic scattering factors taken from Cromer–Liberman tables (Cromer & Liberman, 1970).

(iii) Calculating the fluorescence intensity $I(E)$ with oscillation structures. The refractive indices with oscillation structures ($\delta_{\rm corr}$, $\beta_{\rm corr}$) are computed using the atomic scattering factors corrected by the correction factor $\alpha(E)$. Then, the layer thickness, density, roughness and the corrected refractive indices are used to calculate $I(E)$ based on the fundamental parameter approach.

(iv) Calculating the true EXAFS function $\chi_{\rm corr}(E)$. The correction factor $\alpha(E)$ is optimized using an iterative procedure by comparing $\chi_{\rm cal}(E) = [I(E) - I_0(E)]/[\Delta I_0(E_0)]$ with the experimental function $\chi_{\rm expt}(E)$. When reaching the convergence, the corrected EXAFS function $\chi_{\rm corr}(E)$ are obtained by $\chi_{\rm expt}(E)[1 + \alpha(E)]$.

The detailed correction procedures are described in the following sections.

Before making corrections on $\chi_{\rm expt}(E)$ data, the model parameters of the sample are required, which can be determined based on XRR fitting results as we did for the Cr/C multilayer. Once the model parameters are determined, the EXAFS function $\chi_{\rm cal}(E)$ is needed to be computed for comparing with the experimental data $\chi_{\rm expt}(E)$ as illustrated in Fig. 5. For calculating $\chi_{\rm cal}(E)$, the fluorescence intensity of $I_0(E)$, $I(E)$ and the jump step of $\Delta I_0(E_0)$ need to be known as given by equation (11). Since $I_0(E)$ represents the normalized fluorescence intensity for an isolated atom, it can be simulated using equation (10) with atomic scattering factors f_0' and f_0'' taken from Cromer–Liberman tables. The other quantities, such as the refractive index (δ_0, β_0) and the absorption coefficient (μ_0) for the isolated atom, can be determined using equations (2) and (3) with the factors f_0' and f_0''. Fig. 6 gives the refractive index δ_0 and β_0 of an isolated Cr atom as a function of X-ray photon energy, which are calculated from the atomic scattering factors f_0' and f_0''. Using these quantities and the model parameters of the sample, the fluorescence intensity $I_0(E)$ without oscillation structures for the isolated atom can be calculated at the EXAFS energy regime using equations (9) and (10). Then, the jump step of $\Delta I_0(E_0)$ at the absorption edge can also be determined using $I_0(E)$.

For calculating the fluorescence intensity $I(E)$ with oscillating structures, anomalous scattering factors $f_{\rm corr}'$ and $f_{\rm corr}''$ at the EXAFS energy regime for the detected atom need to be estimated. For other elements of the sample components different from the detected one, the atomic scattering factors f_0' and f_0'' without oscillation structures can still be used.

According to equation (3), the absorption coefficient μ is proportional to the scattering factor f''. So, the corrected scattering factor $f''_{\rm corr}$ can be estimated using the following relation,

$$f''_{\rm corr}(E) = f''_0(E)\{1 + \chi_{\rm expt}(E)[1 + \alpha(E)]\}. \quad (13)$$

Here $\chi_{\rm expt}(E)$ is extracted from EXAFS experimental results and the correction factor $\alpha(E)$ can be assumed to be zero as initial values. Instead of using $\alpha(E) = 0$, another way to properly estimate the initial values of $\alpha(E)$ is to calculate $\chi_{\rm cal}(E)$ using $f''_{\rm corr} = f''_0[1 + \chi_{\rm expt}(E)]$. Then the initial values of $\alpha(E)$ can be estimated as $\chi_{\rm expt}(E)/\chi_{\rm cal}(E) - 1$. This optimization method for estimating the initial values of $\alpha(E)$ greatly reduces the computation time and improves the convergence speed.

Besides the factor $f''_{\rm corr}$, another scatting factor $f'_{\rm corr}$ is also required for calculating the fluorescence intensity, which can be quantified by using the Kramers–Kronig relation

$$f'(E) = \frac{2}{\pi} P \int_0^\infty \frac{E' f''(E')}{E^2 - E'^2} \, {\rm d}E', \quad (14)$$

where P is the Cauchy principal value. In this study, the *DIFFKK* algorithm was used to determine $f'_{\rm corr}$ at the corresponding photon energy *via* Kramers–Kronig transform (Cross *et al.*, 1998). During the iterative procedure, it should be noted that the fine structures in $f''_{\rm corr}(E)$ can influence the values of $f'_{\rm corr}(E)$ according to equation (14). Therefore, if the initial values of $\alpha(E)$ cannot be given properly, more iterative procedures may be needed to reach the final convergent values of $\alpha(E)$. After obtaining the scattering factors $f'_{\rm corr}(E)$ and $f''_{\rm corr}(E)$, the real and imaginary part of the corrected refractive index, *i.e.* $\delta_{\rm corr}$ and $\beta_{\rm corr}$, as well as the absorption coefficient $\mu_{\rm corr}$, are thus obtained using equations (2) and (3). In Fig. 6, the finally optimized refractive index of $\delta_{\rm corr}(E)$ and $\beta_{\rm corr}(E)$ are given for the detected Cr atom in the Cr/C multilayer sample, where the structure in $\delta_{\rm corr}(E)$ is found to be $\sim\pi/2$ out of phase with that of $\beta_{\rm corr}(E)$. For the sake of clarity, we show in Fig. 6 only the refractive index determined from the EXAFS data at the angle of $\theta = 3°$, but the indices obtained from other angles are almost identical to the others after correction. Based on the quantities ($\delta_{\rm corr}$, $\beta_{\rm corr}$ and $\mu_{\rm corr}$) and the model parameters of the multilayer, the fluorescence intensity $I(E)$ with oscillating structures are calculated using the formalism given in §3. After obtaining the fluorescence intensity with and without oscillating structures, $\chi_{\rm cal}(E)$ is obtained using the relation $\chi_{\rm cal}(E) = [I(E) - I_0(E)]/[\Delta I_0(E_0)]$ as shown in Fig. 5. By comparing $\chi_{\rm cal}(E)$ with the experimental data $\chi_{\rm expt}(E)$, the correction factor $\alpha(E)$ can be optimized by an iterative procedure until the best values are obtained. The finally optimized correction factors for the EXAFS spectra of the Cr/C multilayer are shown in the supporting information (Fig. S1).[1] When the convergence has been reached, the corrected EXAFS signal $\chi_{\rm corr}(E)$ can be finally obtained as $\chi_{\rm expt}(E)[1 + \alpha(E)]$.

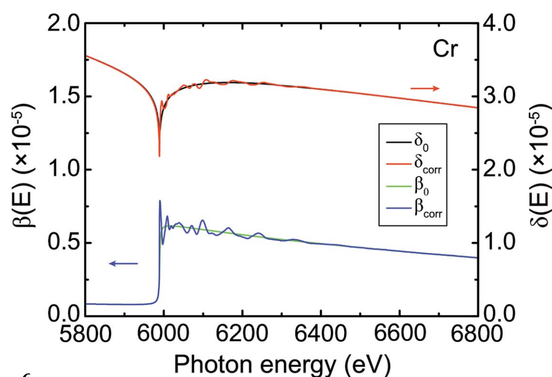

Figure 6
Calculated refractive index of δ_0 and β_0 for the isolated Cr atom and the corrected refractive index of $\delta_{\rm corr}$ and $\beta_{\rm corr}$ for the Cr layer medium in the Cr/C multilayer sample.

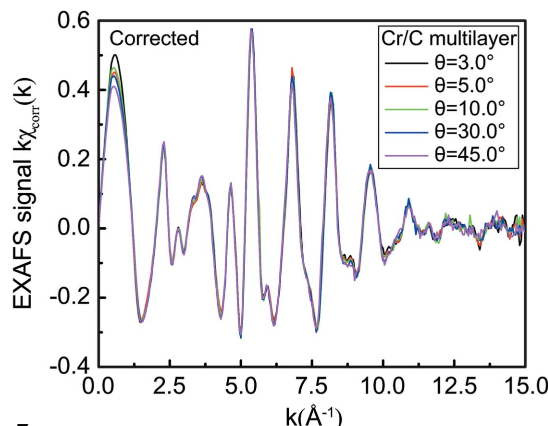

Figure 7
Corrected EXAFS signal $k\chi_{\rm corr}(k)$ for the Cr/C multilayer sample after having applied the correction procedures.

After making corrections on the measured spectra, the corrected EXAFS data for the Cr/C multilayer are shown in Fig. 7 for different experimental geometries. As expected, all the corrected EXAFS signals are in good agreement with each other within noise, which proves the validity of this correction method. The distinct differences between the corrected spectra in the region of k < 1.0 Å^{-1} are probably due to the improperly defined background function or the refractive index, which are difficult to determine in the absorption edge region. In order to avoid the edge effect, the corrected data could be truncated at the low k region, which is typically set at 2 Å^{-1}.

5. Conclusion

In this study, a novel correction method based on the formalism of fluorescence intensity calculation is proposed to correct the self-absorption effects for single-layer or multilayer samples in fluorescence EXAFS experiments. This correction method takes into account the effects of refraction and multiple reflection between neighboring layers, which have been ignored in previous correction methods because of the very simple formula used. This correction method has been tested on the EXAFS spectra of a [Cr(20.08 nm)/

[1] Supporting information for this paper is available from the IUCr electronic archives (Reference: HF5245).

$C(10.63\,nm)]_5$ multilayer sample measured at different experimental geometries, where the damping of the EXAFS amplitudes caused by the self-absorption effects is clearly observed in the uncorrected spectra. After making corrections, almost identical EXAFS spectra have been obtained within noise, which proves the validity of this method.

In principle, this correction method can be applied to any single-layer or multilayer films without thickness limit, when the model parameters of samples with flat surfaces are known. The correction procedure is made in k-space at the beginning before any further data analysis on EXAFS data. This method may also be used as an approach to estimate the influence of self-absorption effects on the amplitudes of EXAFS signals. For the application of the fluorescence EXAFS approach on characterizing local atomic structures for multilayer samples with a depth resolution, this correction method has the potential to be widely used because these experiments based on X-ray standing waves (Meyer *et al.*, 2000) are usually performed with variable incidence angles in order to fix the positions of X-ray probes.

This research has been supported by the 973 program (grant No. 2011CB922203), the National Nature Science Foundation of China (grant Nos. 11075118, 11027507), the Specialized Research Fund for the Doctoral Program of Higher Education (grant No. 20100072120036) and Fundamental Research Funds for the Central Universities. The authors thank beamline BL14W1 (Shanghai Synchrotron Radiation Facility) for providing the beam time.

References

Achkar, A. J., Regier, T. Z., Wadati, H., Kim, Y. J., Zhang, H. & Hawthorn, D. G. (2011). *Phys. Rev. B*, **83**, 081106.
BL14W1@SSRF (2009). *BL14W1 – X-ray Absorption Fine Structure Spectroscopy*, http://ssrf.sinap.ac.cn/english/3/BL14W1.htm.
Boer, D. K. G. de (1991). *Phys. Rev. B*, **44**, 498–511.
Booth, C. H. & Bridges, F. (2005). *Phys. Scr.* T**115**, 202–204.
Brewe, D. L., Pease, D. M. & Budnick, J. I. (1994). *Phys. Rev. B*, **50**, 9025–9030.
Carboni, R., Giovannini, S., Antonioli, G. & Boscherini, F. (2005). *Phys. Scr.* T**115**, 986–988.
Castañer, R. & Prieto, C. (1997). *J. Phys. III Fr.* **7**, 337–349.
Cromer, D. T. & Liberman, D. (1970). *J. Chem. Phys.* **53**, 1891–1898.
Cross, J. O., Newville, M., Rehr, J. J., Sorensen, L. B., Bouldin, C. E., Watson, G., Gouder, T., Lander, G. H. & Bell, M. I. (1998). *Phys. Rev. B*, **58**, 11215–11225.
Eisebitt, S., Böske, T., Rubensson, J. E. & Eberhardt, W. (1993). *Phys. Rev. B*, **47**, 14103–14109.
Ghose, S. K. & Dev, B. N. (2001). *Phys. Rev. B*, **63**, 245409.
Hayakawa, S., Gohshi, Y., Iida, A., Aoki, S. & Sato, K. (1991). *Rev. Sci. Instrum.* **62**, 2545–2549.
Heald, S. M., Chen, H. & Tranquada, J. M. (1988). *Phys. Rev. B*, **38**, 1016–1026.
Henke, B. L., Gullikson, E. M. & Davis, J. C. (1993). *At. Data Nucl. Data Tables*, **54**, 181–342.
Jaklevic, J., Kirby, J. A., Klein, M. P., Robertson, A. S., Brown, G. S. & Eisenberger, P. (1977). *Solid State Commun.* **23**, 679–682.
Jiang, D. T. & Crozier, E. D. (1998). *Can. J. Phys.* **76**, 621–643.
Li, W., Zhu, J., Ma, X., Li, H., Wang, H., Sawhney, K. J. & Wang, Z. (2012). *Rev. Sci. Instrum.* **83**, 053114.
Meirer, F., Pepponi, G., Streli, C., Wobrauschek, P., Kregsamer, P., Zoeger, N. & Falkenberg, G. (2008). *Spectrochim. Acta B*, **63**, 1496–1502.
Meyer, D. C., Holz, T., Krawietz, R., Richter, K., Wehner, B. & Paufler, P. (1995). *Phys. Status Solidi A*, **150**, 603–612.
Meyer, D. C., Richter, K., Paufler, P., Gawlitza, P. & Holz, T. (2000). *J. Appl. Phys.* **87**, 7218–7226.
Parratt, L. G. (1954). *Phys. Rev.* **95**, 359–369.
Pease, D. M., Brewe, D. L., Tan, Z., Budnick, J. I. & Law, C. C. (1989). *Phys. Lett. A*, **138**, 230–234.
Pfalzer, P., Urbach, J. P., Klemm, M., Horn, S., denBoer, M. L., Frenkel, A. I. & Kirkland, J. P. (1999). *Phys. Rev. B*, **60**, 9335.
Ravel, B. & Newville, M. (2005). *J. Synchrotron Rad.* **12**, 537–541.
Suzuki, Y. (1989). *Phys. Rev. B*, **39**, 3393–3395.
Tan, Z., Budnick, J. I. & Heald, S. M. (1989). *Rev. Sci. Instrum.* **60**, 1021–1025.
Tiwari, M. K., Lodha, G. S. & Sawhney, K. J. S. (2010). *X-ray Spectrom.* **39**, 127–134.
Tröger, L., Arvanitis, D., Baberschke, K., Michaelis, H., Grimm, U. & Zschech, E. (1992). *Phys. Rev. B*, **46**, 3283.
Windt, D. L. (1998). *Comput. Phys.* **12**, 360–370.
Wormington, M., Panaccione, C., Matney, K. M. & Bowen, D. K. (1999). *Philos. Trans. R. Soc. London A*, **357**, 2827–2848.